RESEARCH ARTICLE | NOVEMBER 19 2024

How dynamic surface restructuring impacts intra-particle catalytic cooperativity

Bhawakshi Punia ; Srabanti Chaudhury ; Anatoly Kolomeisky

J. Chem. Phys. 161, 194107 (2024)
https://doi.org/10.1063/5.0239455

The Journal of Chemical Physics ARTICLE pubs.aip.org/aip/jcp

How dynamic surface restructuring impacts intra-particle catalytic cooperativity

Cite as: J. Chem. Phys. 161, 194107 (2024); doi: 10.1063/5.0239455
Submitted: 19 September 2024 • Accepted: 31 October 2024 •
Published Online: 19 November 2024

Bhawakshi Punia,[1] Srabanti Chaudhury,[1,a)] and Anatoly Kolomeisky[2,a)]

AFFILIATIONS

[1] Department of Chemistry, Indian Institute of Science Education and Research, Dr. Homi Bhabha Road, Pune 411008, Maharashtra, India

[2] Department of Chemistry, Department of Chemical and Biomolecular Engineering, Department of Physics and Astronomy, and Center for Theoretical Biological Physics, Rice University, 6100 Main Street, Houston, Texas 77005, USA

[a)] **Authors to whom correspondence should be addressed:** srbanti@iiserpune.ac.in and tolya@rice.edu

ABSTRACT

Recent experiments indicated that nanoparticles (NPs) might efficiently catalyze multiple chemical reactions, frequently exhibiting new phenomena. One of those surprising observations is intra-particle catalytic cooperativity, when the reactions at one active site can stimulate the reactions at spatially distant sites. Theoretical explanations of these phenomena have been presented, pointing out the important role of charged hole dynamics. However, the crucial feature of nanoparticles that can undergo dynamic structural surface rearrangements, potentially affecting the catalytic properties, has not yet been accounted for. We present a theoretical study of the effect of dynamic restructuring in NPs on intra-particle catalytic cooperativity. It is done by extending the original static discrete-state stochastic framework that quantitatively evaluates the catalytic communications. The dynamic restructuring is modeled as stochastic transitions between states with different dynamic properties of charged holes. Our analysis reveals that the communication times always decrease with increasing rates of dynamic restructuring, while the communication lengths exhibit a dynamic behavior that depends on how dynamic fluctuations affect migration and death rates of charged holes. Computer simulations fully support theoretical predictions. These findings provide important insights into the microscopic mechanisms of catalysis on single NPs, suggesting specific routes to rationally design more efficient catalytic systems.

I. INTRODUCTION

Catalysis accelerates chemical reactions by using specific compounds, called catalysts, that are not consumed by these reactions, providing alternate pathways to increase the rates of these processes.[1] It is widely explored, ranging from living systems to various modern industries, affecting a huge number of important phenomena.[2,3] Recent experimental efforts led to the introduction of metal-based nanoparticles (NPs) as novel heterogeneous catalysts for complex processes where the reactants, catalysts, and products might exist in distinct thermodynamic phases.[4–8] The advantage of NPs as catalysts is that they can be synthesized in various specific shapes, sizes, and chemical compositions, providing better control for the outcome of catalyzed chemical reactions.[9–11]

The application of NPs also allowed the catalytic processes to be investigated with more quantitative details by using a variety of novel single-molecule approaches with high spatial and temporal resolutions, clarifying many aspects of underlying molecular mechanisms.[12–16] Several new phenomena related to catalysis have been discovered.[17] One of the most surprising of them is the observation of intra-particle catalytic cooperativity.[18] It was found that during the catalysis of redox chemical reactions on *Au* and *Pd* nanoparticles, the processes at some active sites stimulated the same processes at the spatially close but distinct active sites. Statistical analysis of Pearson's cross correlation coefficients (PCCs) between different segments of individual nanoparticles revealed that successive product-formation events were correlated with a temporal memory (or lifetime) of ~10–100 s and a communication distance of ~200–600 nm.[18] Such cooperative communications are reminiscent of the allosteric effects observed in proteins, but their molecular origins are completely different.[19] Experiments also identified the positively charged holes moving on the oxidized surfaces of metal NPs as being responsible for the observed catalytic cooperativity.[18]

To explain these surprising observations, we recently developed a novel theoretical framework to clarify the microscopic picture of catalytic cooperativity.[20] It was proposed that the probability of the catalytic reaction taking place at a given active site depends on the local concentration of positively charged holes, and each redox reaction creates an additional amount of charged holes.[21–23] Then, a higher local concentration of charge holes after the reaction took place at the given active site drives them away to other parts of the nanoparticle with lower concentrations of charged holes, increasing the pool of charged holes near neighboring active sites. This eventually stimulates new chemical reactions at these new sites. Based on this hypothesis, we developed a discrete-state stochastic model that allowed us to obtain a comprehensive description of catalytic cooperativity processes.[20] The proposed theoretical approach gave excellent quantitative agreements with experimentally observed ranges of communication distances and temporal memories and the dependence on the external fields, explaining the universality of catalytic cooperative effects and clarifying several mechanistic aspects of the phenomenon. It was later extended to account for the possible spatial heterogeneity of nanocatalysts,[24] predicting that spatial heterogeneity should decrease communication distances and temporal memories while simultaneously increasing the strength of correlations.

While the proposed theoretical framework successfully captured most of the features of catalytic cooperativity, it neglected an important property of nanoparticles. The theoretical method assumed that the structures of nanoparticles are always static, i.e., that their catalytic properties do not change over time. However, there are multiple experimental observations of temporal fluctuations of metal NPs, which are frequently manifested through dynamic surface restructuring.[25,26] It was shown, for example, that *Au* nanoparticles that participate in catalytic hydrogenation experience significant size- and shape-dependent transformations, switching between so-called resting and active states.[27] A size-dependent restructuring of *Ni* nanoparticles has also been observed.[28] In addition, recent kinetic Monte Carlo simulation studies have shown that such dynamic reshaping of nanocatalysts may lead to changes in the active sites, which can eventually influence the overall catalytic efficiency.[29] Furthermore, these fluctuations can be induced by substrate molecules adsorbed on the nanocatalyst's surfaces.[30] The dynamic restructuring might also arise from various environmental factors that eventually impact the catalytic efficiency of the metal NPs.[31] It is critically important to understand how such dynamic fluctuations of nanoparticle surfaces can influence the underlying microscopic mechanisms of catalysis, especially when the involved active sites can communicate with each other at the intra-particle level. However, the corresponding theoretical method to quantify such effects is currently missing.

In this work, a theoretical investigation of the effect of dynamic restructuring of NPs on the intra-particle catalytic cooperativity is presented. We extend the original static stochastic framework and consider dynamic fluctuations as transformations between different macroscopic states that exhibit different dynamic properties of charged holes. This allows us to obtain an explicit description of the catalytic cooperativity phenomena in the presence of dynamic fluctuations. Analytical calculations are supported by Monte Carlo computer simulations. We also present physical–chemical arguments to explain the theoretical predictions. Our theoretical study uncovers novel microscopic features of catalytic phenomena, opening the possibilities for rationally designing optimal catalytic systems.

II. THEORETICAL MODEL

To explain our theoretical method, let us consider a single nanoparticle that can catalyze only one type of redox chemical reaction, as shown schematically in Fig. 1. Because experimental studies are mostly focused on nanorods, we adopt an effective one-dimensional description of catalytic processes,[18] although the method can be extended to more complex geometries of NPs. In our theoretical approach, the lattice with several segments each of

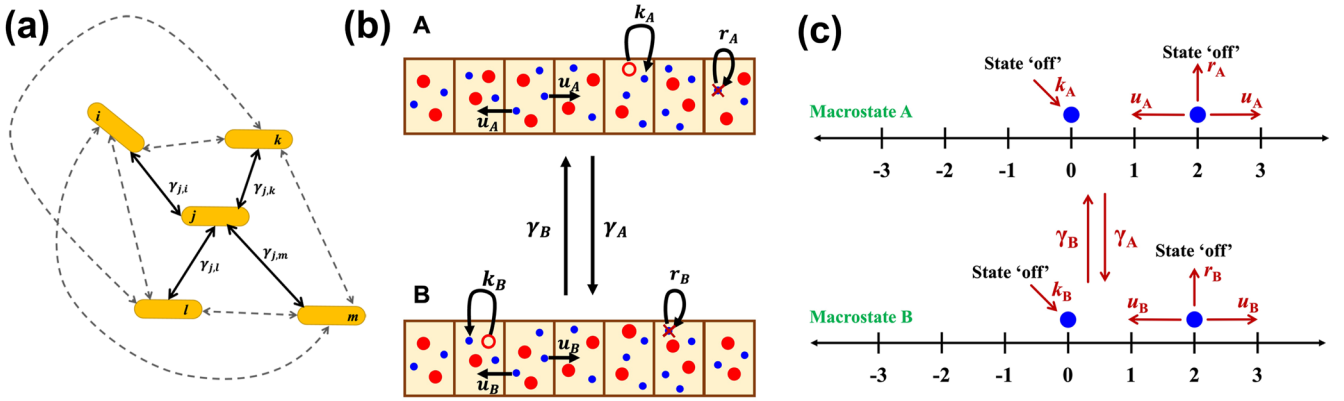

FIG. 1. (a) A schematic representation of dynamic restructuring in the single NP, which is viewed as a network of macroscopic states and transitions between them. (b) A simple case when the nanorod fluctuates only between two macroscopic states, *A* and *B*. The rates γ_A and γ_B describe the corresponding transitions. The nanorod is divided into multiple segments of equal length, possessing a uniform distribution of active sites (red-filled circles) that produce charged holes (blue circles) while catalyzing redox reactions. A new charged hole appears with the rate $k_{j=A,B}$ at a given active site (empty red circle) of the nanorod. For any macrostate *A* (or *B*), charged holes migrate to adjacent segments with the rate u_A (or u_B), and they can also disappear from a segment with the rate r_A (or r_B). (c) A corresponding discrete-state stochastic model to describe a dynamically fluctuating nanorod. The states $n = 0, \pm1, \pm2, \ldots$ represent the different nanorod segments after a new hole is produced at state $n = 0$ at some initial time.

length l represents the single nanorod with multiple active sites. For simplicity, we also assume that the number of active sites per segment is the same, but the analysis for spatially heterogeneous cases is also possible.[20,24] It has been proposed earlier, using experimental observations and theoretical arguments, that due to the nature of redox reactions, charged holes play a critical role in the mechanisms of catalytic cooperativity.[18,20] More specifically, in our original theoretical framework, we assumed that each reaction at the active site might create new charged holes.[20] The charged holes can then migrate between different parts of the nanorod, and they can also disappear from the system.

To account for dynamic restructuring, we postulate that these fluctuations lead to different macroscopic states that exhibit different diffusion and death rates of charged holes. In the macroscopic state j, the charged holes are created with a rate k_j, a migration rate u_j, and a death rate r_j. As shown in Fig. 1(a), these stochastic fluctuations correspond to transitions between different macroscopic states i and j of the system with rates γ_{ij} $(i \to j)$ and γ_{ji} $(j \to i)$. Thus, the dynamic restructuring of the nanorod can be viewed as a network of stochastic transitions, as shown schematically in Fig. 1(a). This allows us to extend the original theoretical framework of analyzing catalytic cooperativity to account also for dynamic fluctuations. In our model, the mean time for the charged hole to stay in the system, which we associate with the communication lifetime, is averaged over all possible macroscopic states. Similarly, the mean distance that the charged particle migrates before disappearing, which we associate with the communication length, is the quantity that is averaged over all possible macrostates.

To understand better the microscopic picture of how dynamic restructuring influences catalytic cooperativity, let us consider the simplest situation when the nanorod can fluctuate only between two macroscopic states labeled A and B. This is shown in Fig. 1(b). The two-macrostate model can be validated from experimental observations. Distinct transitions between resting and active states have been observed, for example, in Au nanoparticles during butadiene hydrogenation,[27] and two types of restructuring processes were also reported on Au nanoparticles while they catalyze the reduction of p-nitrophenol.[30] From state A, the system can change to state B with a rate γ_A, while the reverse transition has a rate γ_B. The charged holes are produced in the macroscopic state A (B) with rate k_A (k_B). These holes might migrate and disappear from the nanorod via the rates u_A (u_B) and r_A (r_B), respectively. To quantify the properties of catalytic cooperativity, we adopt an effective discrete-state stochastic model presented in Fig. 1(c), where one can monitor the fate of a single charged hole on an infinitely long, dynamically fluctuating nanorod. When a new hole is produced on the nanorod in any macrostate with the rate k_A or k_B, we label this segment as the state $n = 0$, and the adjacent segments are labeled as $n = \pm 1, \pm 2, \ldots$ accordingly. This can be done because of the translational symmetry of the system. Since the hole's dynamics are different in each macroscopic state due to the associated transition rates, we adopt a first-passage approach to accurately evaluate the complex details of the catalytic cooperativity dynamics in this system.

To determine the overall lifetime of the charged hole after it is produced at state 0, we consider all the situations for the hole disappearing from each macrostate separately. One can introduce $F^A_{n,j}(t)$ and $F^B_{n,j}(t)$ as the first-passage distribution functions for the hole to disappear from the macrostate A or B, respectively, at time t if it was initially in the segment $-L \le n \le L$ $(L \gg 1)$, or the state $n = off$ if the hole is not yet produced on the lattice, starting in the macrostate $j = A, B$. Let us first analyze the situation when the hole disappears from the macrostate A only. The temporal evolution of the first-passage probabilities $F^A_{n,j}(t)$ can be described via a set of backward master equations. For segment $n = 0$, using the symmetry arguments $F^A_{n,j}(t) = F^A_{-n,j}(t)$, we have

$$\frac{dF^A_{0,A}(t)}{dt} = 2u_A F^A_{1,A}(t) + r_A F^A_{d,A}(t) + \gamma_A F^A_{0,B}(t) - (2u_A + r_A + \gamma_A) F^A_{0,A}(t), \tag{1a}$$

$$\frac{dF^A_{0,B}(t)}{dt} = 2u_B F^A_{1,B}(t) + \gamma_B F^A_{0,A}(t) - (2u_B + r_B + \gamma_B) F^A_{0,B}(t). \tag{1b}$$

Here, we use $F^A_{d,A}(t) = \delta(t)$ as the initial condition, which suggests that the hole at $t = 0$ has already dissociated from the lattice in the macrostate A, and the process ends immediately. The above equations also ensure that the hole will disappear only from the macrostate A. For segments $n \neq 0, \pm L$, one can write

$$\frac{dF^A_{n,A}(t)}{dt} = u_A F^A_{n-1,A}(t) + u_A F^A_{n+1,A}(t) + r_A F^A_{d,A}(t) + \gamma_A F^A_{n,B}(t) - (2u_A + r_A + \gamma_A) F^A_{n,A}(t), \tag{2a}$$

$$\frac{dF^A_{n,B}(t)}{dt} = u_B F^A_{n-1,B}(t) + u_B F^A_{n+1,B}(t) + \gamma_B F^A_{n,A}(t) - (2u_B + r_B + \gamma_B) F^A_{n,B}(t). \tag{2b}$$

For the lattice ends, $F^A_{L,j}(t) = F^A_{-L,j}(t)$, we have

$$\frac{dF^A_{L,A}(t)}{dt} = u_A F^A_{L-1,A}(t) + r_A F^A_{d,A}(t) + \gamma_A F^A_{L,B}(t) - (u_A + r_A + \gamma_A) F^A_{L,A}(t), \tag{3a}$$

$$\frac{dF^A_{L,B}(t)}{dt} = u_B F^A_{L-1,B}(t) + \gamma_B F^A_{L,A}(t) - (u_B + r_B + \gamma_B) F^A_{L,B}(t). \tag{3b}$$

In addition, for the state "off," the backward master equations are written as

$$\frac{dF^A_{off,A}(t)}{dt} = k_A F^A_{0,A}(t) + \gamma_A F^A_{off,B}(t) - (k_A + \gamma_A) F^A_{off,A}(t), \tag{4a}$$

$$\frac{dF^A_{off,B}(t)}{dt} = k_B F^A_{0,B}(t) + \gamma_B F^A_{off,A}(t) - (k_B + \gamma_B) F^A_{off,B}(t). \tag{4b}$$

It is convenient to solve the above backward master equations in the Laplace space, $\tilde{F}^A_{n,j}(s) = \int_0^\infty F^A_{n,j}(t) e^{-st}$, allowing us to rewrite Eqs. (1)–(4) as

$$(s + 2u_A + r_A + \gamma_A)\tilde{F}^A_{0,A}(s) = 2u_A \tilde{F}^A_{1,A}(s) + r_A + \gamma_A \tilde{F}^A_{0,B}(s), \tag{5a}$$

$$(s + 2u_B + r_B + \gamma_B)\tilde{F}^A_{0,B}(s) = 2u_B \tilde{F}^A_{1,B}(s) + \gamma_B \tilde{F}^A_{0,A}(s) \tag{5b}$$

for the state $n = 0$, and for $n \neq 0$ and $n \neq \pm L$, we have

$$(s + 2u_A + r_A + \gamma_A)\tilde{F}^A_{n,A}(s) = u_A \tilde{F}^A_{n-1,A}(s) + u_A \tilde{F}^A_{n+1,A}(s) + r_A + \gamma_A \tilde{F}^A_{n,B}(s), \tag{6a}$$

$$(s+2u_B+r_B+\gamma_B)\tilde{F}^A_{n,B}(s)=u_B\tilde{F}^A_{n-1,B}(s)+u_B\tilde{F}^A_{n+1,B}(s)+\gamma_B\tilde{F}^A_{n,A}(s). \tag{6b}$$

For the ends of the nanorod, $n = L$, one can write

$$(s+u_A+r_A+\gamma_A)\tilde{F}^A_{L,A}(s)=u_A\tilde{F}^A_{L-1,A}(s)+r_A+\gamma_A\tilde{F}^A_{L,B}(s), \tag{7a}$$

$$(s+u_B+r_B+\gamma_B)\tilde{F}^A_{L,B}(s)=u_B\tilde{F}^A_{L-1,B}(s)+\gamma_B\tilde{F}^A_{L,A}(s). \tag{7b}$$

Finally, for the state "off," we write the Laplace transformed backward master equations as

$$(s+k_A+\gamma_A)\tilde{F}^A_{off,A}(s)=k_A\tilde{F}^A_{0,A}(s)+\gamma_A\tilde{F}^A_{off,B}(s), \tag{8a}$$

$$(s+k_B+\gamma_B)\tilde{F}^A_{off,B}(s)=k_B\tilde{F}^A_{0,B}(s)+\gamma_B\tilde{F}^A_{off,A}(s). \tag{8b}$$

The explicit expressions for the functions $F^A_{0,j=A,B}(t)$ can be obtained by solving the above set of equations as shown in the supplementary material,

$$\tilde{F}^A_{0,A}(s)=\frac{r_A(\phi_B-2u_B)}{\phi_1-2\phi_2+2\phi_3}, \tag{9a}$$

$$\tilde{F}^A_{0,B}(s)=\frac{r_A\gamma_B}{\phi_1-2\phi_2+2\phi_3}, \tag{9b}$$

where

$$\phi_1(s)=\phi_A\phi_B+2u_Au_B-\gamma_A\gamma_B,\quad \phi_2(s)=u_A\phi_B+u_B\phi_A,\quad \phi_3=u_Au_B, \tag{10}$$

and $\phi_{j=A,B}(s)=s+2u_j+r_j+\gamma_j$.

A similar set of calculations can be performed for the first-passage distribution functions $F^B_{n,j}(t)$. In the Laplace transformed space, the final results are

$$\tilde{F}^B_{0,A}(s)=\frac{r_B\gamma_A}{\phi_1-2\phi_2+2\phi_3}, \tag{11a}$$

$$\tilde{F}^B_{0,B}(s)=\frac{r_B(\phi_A-2u_A)}{\phi_1-2\phi_2+2\phi_3}. \tag{11b}$$

Equations (9)–(11) are the main results of this work. This is because these first-passage distribution functions can now be fully analyzed, and one can determine all characteristic features of the catalytic cooperativity. We are specifically interested in evaluating the communication lifetimes and lengths, as explained in Sec. III.

III. RESULTS AND DISCUSSION

To understand better the role of dynamic restructuring, one has to compare the properties of catalytic cooperativity for dynamically fluctuating systems with those for homogeneous non-fluctuating systems. For this purpose, we introduce dimensionless heterogeneity parameters α_u and α_r defined as

$$u_A=\alpha_u u,\quad u_B=\frac{u}{\alpha_u};\quad r_A=\alpha_r r,\quad r_B=\frac{r}{\alpha_r}, \tag{12}$$

where the rates u and r correspond to a purely homogeneous case without dynamic fluctuations.[20] Thus, by varying these parameters, one can see the continuous changes in the catalytic cooperativity induced by dynamic restructuring. It is important to note here that this is not the only way to probe the effect of dynamic fluctuations since the migration and death rates could have more complex dependencies. However, this is the simplest convenient approach with a minimal number of variables that should allow us to explain more clearly the physics of these complex phenomena. In addition, to simplify calculations, in most situations, we assume that fluctuation rates between different macroscopic states are the same, $\gamma_A = \gamma_B = \gamma$, although our analysis is valid for more general situations.

A. Communication lifetime or temporal memory

Now let us explicitly evaluate the temporal memory in catalytic cooperativity for the systems that experience dynamic restructuring. It corresponds to the average time a charged hole stays on the nanorod after it was initially produced. Using our analysis and the results in Eq. (9), the splitting probabilities ($\Pi^A_{0,j=A,B}$) and the mean first-passage times ($T^A_{0,j=A,B}$) for the charged hole to disappear only from the macrostate A after it was initially produced in segment 0 on the nanorod can be estimated as

$$\Pi^A_{0,A}=\tilde{F}^A_{0,A}(s=0)=\frac{r_A(\gamma_B+r_B)}{r_A\gamma_B+r_B\gamma_A+r_Ar_B}, \tag{13a}$$

$$\Pi^A_{0,B}=\tilde{F}^A_{0,B}(s=0)=\frac{r_A\gamma_B}{r_A\gamma_B+r_B\gamma_A+r_Ar_B}, \tag{13b}$$

$$T^A_{0,A}=-\frac{\partial_s\tilde{F}^A_{0,A}(s=0)}{\Pi^A_{0,A}}=\frac{\gamma_A\gamma_B+(\gamma_B+r_B)^2}{(\gamma_B+r_B)(r_A\gamma_B+r_B\gamma_A+r_Ar_B)}, \tag{13c}$$

$$T^A_{0,B}=-\frac{\partial_s\tilde{F}^A_{0,B}(s=0)}{\Pi^A_{0,B}}=\frac{\gamma_A+\gamma_B+r_A+r_B}{r_A\gamma_B+r_B\gamma_A+r_Ar_B}. \tag{13d}$$

Using a similar strategy for Eq. (11), one can determine the respective splitting probabilities ($\Pi^B_{0,j=A,B}$) and mean first-passage times ($T^B_{0,j=A,B}$) for the hole to disappear only from the macrostate B after it is produced in the segment 0 of the nanorod. These quantities are

$$\Pi^B_{0,A}=\tilde{F}^B_{0,A}(s=0)=\frac{r_B\gamma_A}{r_A\gamma_B+r_B\gamma_A+r_Ar_B}, \tag{14a}$$

$$\Pi^B_{0,B}=\tilde{F}^B_{0,B}(s=0)=\frac{r_B(\gamma_A+r_A)}{r_A\gamma_B+r_B\gamma_A+r_Ar_B}, \tag{14b}$$

$$T^B_{0,A}=-\frac{\partial_s\tilde{F}^B_{0,A}(s=0)}{\Pi^B_{0,A}}=\frac{\gamma_A+\gamma_B+r_A+r_B}{r_A\gamma_B+r_B\gamma_A+r_Ar_B}, \tag{14c}$$

$$T^B_{0,B}=-\frac{\partial_s\tilde{F}^B_{0,B}(s=0)}{\Pi^B_{0,B}}=\frac{\gamma_A\gamma_B+(\gamma_A+r_A)^2}{(\gamma_A+r_A)(r_A\gamma_B+r_B\gamma_A+r_Ar_B)}. \tag{14d}$$

Finally, the overall mean lifetime (τ) of the charged hole can be calculated by averaging over all possible initial states and all possible macrostates from which it disappears,[32]

$$\tau=\frac{P_A\left(\Pi^A_{0,A}T^A_{0,A}+\Pi^B_{0,A}T^B_{0,A}\right)+P_B\left(\Pi^A_{0,B}T^A_{0,B}+\Pi^B_{0,B}T^B_{0,B}\right)}{P_A\left(\Pi^A_{0,A}+\Pi^B_{0,A}\right)+P_B\left(\Pi^A_{0,B}+\Pi^B_{0,B}\right)}. \tag{15}$$

In these expressions, we defined $P_A = \gamma_B/(\gamma_A + \gamma_B)$ and $P_B = \gamma_A/(\gamma_A + \gamma_B)$ as the steady-state probabilities for the nanorod to exist in the macrostates A and B, respectively. The steady-state calculations are provided in the supplementary material. By substituting Eqs. (13) and (14) into Eq. (15), we obtain the overall temporal memory of catalytic cooperativity,

$$\tau = \frac{r_A\gamma_A + r_B\gamma_B + (\gamma_A + \gamma_B)^2}{(\gamma_A + \gamma_B)(r_A\gamma_B + r_B\gamma_A + r_A r_B)}. \tag{16a}$$

If the fluctuation rates are equal, $\gamma_A = \gamma_B = \gamma$, the lifetime simplifies into

$$\tau = \frac{r_A + r_B + 4\gamma}{2[r_A r_B + \gamma(r_A + r_B)]}. \tag{16b}$$

Note that the cooperativity lifetime is independent of the diffusion rates u_A and u_B. Using the relations from Eq. (12), the lifetimes can be rewritten as

$$\tau = \frac{r(\alpha_r + \alpha_r^{-1}) + 4\gamma}{2r\left[r + \gamma(\alpha_r + \alpha_r^{-1})\right]}. \tag{16c}$$

When the dynamic restructuring does not affect the death rates, $\alpha_r = 1$, it can be shown that Eq. (16c) reduces to $\tau = 1/r$, which, as expected, fully agrees with the estimates of the communication lifetimes for homogeneous nanorods.[20] In the case when the dynamic restructuring is very slow, Eq. (16c) reduces to

$$\tau(\gamma \to 0) \simeq \frac{1}{2}\left(\frac{1}{r\alpha_r} + \frac{1}{r/\alpha_r}\right), \tag{17}$$

while in the limit of very fast dynamic fluctuations we obtain

$$\tau(\gamma \to \infty) \simeq \frac{1}{r\left(\alpha_r + \frac{1}{\alpha_r}\right)/2}. \tag{18}$$

These results can be explained using the following arguments: When the dynamic restructuring transitions are rare $(\gamma \to 0)$, the system has enough time to explore both macroscopic states, and the overall communication lifetime can be viewed as average over the macrostates A and B. This means that $\tau = (\tau_A + \tau_B)/2$, where $\tau_A = \frac{1}{r\alpha_r}$ is the temporal memory for the macrostate A and $\tau_B = \frac{1}{r/\alpha_r}$ is the temporal memory for the macrostate B. When the dynamic transitions are very fast $(\gamma \to \infty)$, the system will reach an effective equilibrium between the two macrostates A and B, and it can be viewed as an effectively homogeneous nanorod with the effective equilibrium death rate given by $r_{eff} = (r\alpha_r + \frac{r}{\alpha_r})/2$. Factor 2 reflects that the nanorod is equally probable to be found in the macrostates A or B because the fluctuation rates are the same in both directions $(\gamma_A = \gamma_B = \gamma)$.

To quantify better how the dynamic restructuring is influencing the temporal memory in catalytic cooperativity in comparison with purely static situations, one can introduce a dimensionless parameter $R(\tau)$ defined as

$$R(\tau) = \frac{\tau(\alpha_r)}{\tau(\alpha_r = 1)} = \frac{4\gamma + r\left(\alpha_r + \alpha_r^{-1}\right)}{2\left[r + \gamma\left(\alpha_r + \alpha_r^{-1}\right)\right]}. \tag{19}$$

It shows quantitatively how the temporal memory in the dynamic restructuring system deviates from the situation for the homogeneous nanorod without dynamic fluctuations. $R(\tau) > 1$ corresponds to the situation when dynamic restructuring increases the communication lifetimes, while $R(\tau) < 1$ describes the opposite effect of decreasing the temporal memory for dynamically fluctuating systems.

The results of analytical calculations and Monte Carlo computer simulations for $R(\tau)$ are presented in Fig. 2. For the fixed value of the parameter α_r, it can be shown that increasing the rate of dynamic fluctuations always decreases the communication lifetime of catalytic cooperativity; see Fig. 2(a). One can also see that $R(\tau) > 1$ for relatively small fluctuation rates, while $R(\tau) < 1$ for large fluctuation rates. This can be explained by noticing that for $\gamma \to 0$, the system has enough time to explore both macrostates, and the macrostate with the lowest death rate is equally probable

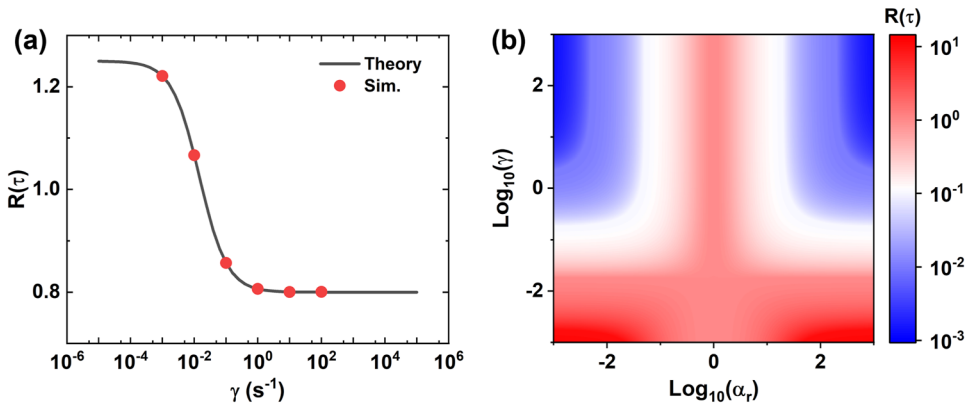

FIG. 2. (a) The ratio $R(\tau)$ plotted as a function of the fluctuation rate γ. Considering $\alpha_r = 2$, the solid black line is obtained analytically, whereas the red symbols correspond to Monte Carlo simulation results. (b) Contour plot for the ratio $R(\tau)$ as a function of rate γ and the dimensionless parameter α_r. Here, $R(\tau)$ is theoretically determined using Eq. (16c), and we used $r = 0.036\,36\ s^{-1}$, which reflects the purely homogeneous death rate of the hole determined for *Pd* nanorod catalyzing resazurin disproportionation.[20] The detailed simulation procedure is explained in the supplementary material.

as the macrostate with the highest death rate. Then the dynamic behavior of the macrostate j with the lowest death rate r_j dominates, and the overall communication times are higher than in the case without fluctuations because the charged hole can stay longer on the nanorod. The situation changes for fast dynamic fluctuations, where the fluctuating system can be effectively mapped into a new homogeneous system with a faster effective death rate [because $(\alpha_r + \frac{1}{\alpha_r})/2$ is always larger than one for $\alpha_r \neq 1$], and this decreases the communication times. One could also estimate the critical value of the fluctuation rate γ_c at which $R(\tau) = 1$. From Eq. (19), it can be shown that $\gamma_c = r/2$. This result suggests that the biggest changes in communication times occur when the fluctuation rates become comparable to the death rates in at least one of the macrostates. This can be seen in Fig. 2(a).

Figure 2(b) illustrates how the parameter $R(\tau)$ generally depends on the fluctuation rate γ and heterogeneity parameter α_r. A complex behavior is observed for different ranges of dynamic fluctuation rates and different heterogeneities. For large γ, the largest communication times [maxima in $R(\tau)$] are observed for the homogeneous system ($\alpha_r = 1$), while for strongly heterogeneous systems ($\alpha_r \to 0$ or $\alpha_r \to \infty$), the communication times always decrease. For small γ, the behavior completely reverses: now, the smallest communication times [minima in $R(\tau)$] are observed for homogeneous systems, while heterogeneous systems exhibit longer communication times. Again, this is the result of different dynamics for slow and fast fluctuation rates, as explained above.

Overall, our theoretical results suggest that for the given set of heterogeneity parameters, communication times generally decrease as a function of the temporal fluctuation rate (γ), i.e., dynamic surface restructuring lowers the temporal memory of catalytic cooperativity. In addition, for the fixed fast fluctuation rates, increasing heterogeneity in death rates (deviating from $\alpha_r = 1$) always lowers the memory lifetimes, while for the fixed slow fluctuation rates, longer communication times are expected for more heterogeneous systems.

B. Communication lengths

As shown in the supplementary material, the average distance traveled by a charged hole on the nanorod can be explicitly evaluated, yielding

$$\lambda = -\frac{l}{\ln x_1}, \tag{20a}$$

where l represents the length of a nanorod segment and the parameter x_1 is given by

$$x_1 = \frac{y_1}{2} - \sqrt{\left(\frac{y_1}{2}\right)^2 - 1}, \tag{20b}$$

with

$$y_1 = \frac{\phi_2(s=0) - \sqrt{\phi_2(s=0)^2 - 4\phi_3(\phi_1(s=0) - 2\phi_3)}}{2\phi_3}. \tag{21}$$

It has been argued before that this length scale can be associated with the communication length of catalytic cooperativity.[20]

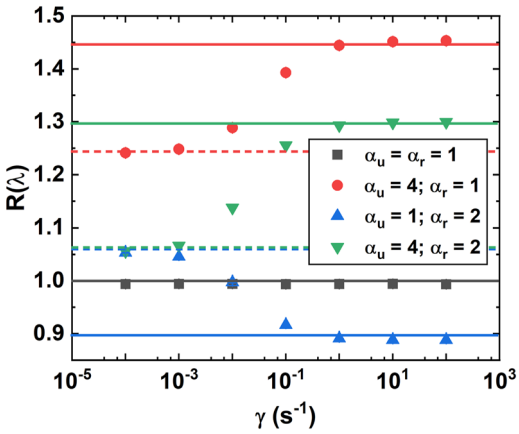

FIG. 3. The ratio $R(\lambda)$ as a function of the fluctuation rate γ for different migration and death rates. For all segments of the length $l = 50$ nm, we used $u = 0.736\ s^{-1}$ and $r = 0.036\,36\ s^{-1}$, which reflect the migration and death rates of the hole determined for a purely homogeneous Pd nanorod catalyzing resazurin disproportionation in Ref. 20. Symbols are Monte Carlo simulation results; dashed lines represent the analytical result obtained for small fluctuation rates using Eq. (28) whereas solid lines are obtained for $\gamma \ll 1$ from Eq. (25). The simulation procedure is explained in the supplementary material.

To better quantify the extent of changes in communication length due to dynamic restructuring, we introduce a dimensionless parameter,

$$R(\lambda) = \frac{\lambda(\alpha_u, \alpha_r)}{\lambda(\alpha_u = \alpha_r = 1)}. \tag{22}$$

It gives a quantitative measure of how much larger the communication length is in the system with dynamic restructuring in comparison with the situation when there are no dynamic fluctuations. For $R(\lambda) > 1$, dynamic restructuring increases the communication length, while for $R(\lambda) < 1$, it makes this length smaller. This quantity, obtained via analytical calculations and computer simulations, is presented in Fig. 3. One can see that for small fluctuation rates, the communication lengths of dynamically restructuring systems ($\alpha_u \neq 1$ and $\alpha_r \neq 1$) are always larger than the corresponding length for the homogeneous system without fluctuations ($\alpha_u = 1$ and $\alpha_r = 1$). However, increasing the fluctuation rate γ has a different effect on the communication lengths depending on explicit values of the heterogeneity parameters α_u and α_r.

These observations can be explained by analyzing the limiting behavior of the system at very fast and very slow structural rearrangements. First, we notice that for homogeneous systems without fluctuations ($\alpha_u = 1$ and $\alpha_r = 1$), the communication length has already been estimated as[20]

$$\lambda(\alpha_u = \alpha_r = 1) \simeq l\sqrt{\frac{u}{r}}. \tag{23}$$

Since for slow dynamic fluctuations ($\gamma \to 0$), the system has enough time to explore both macrostates, the communication length in this limit can be viewed as an average of communication lengths in each macrostate, leading to

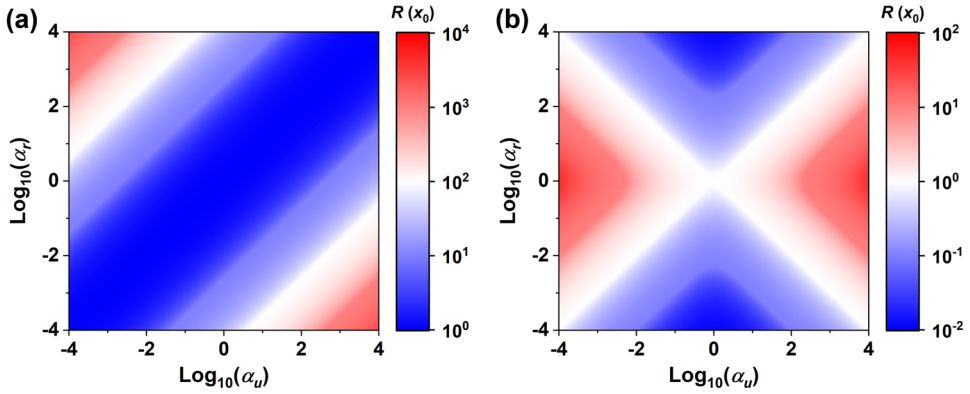

FIG. 4. Contour plots of the ratio $R(\lambda)$ as the function of dimensionless parameters α_u and α_r when the fluctuation rates between the macrostates are (a) very slow [$\gamma = 10^{-3}$ and calculations done using Eq. (25)] and (b) very fast [$\gamma = 10^{2}$ and calculations done using Eq. (28)].

$$\lambda(\gamma \to 0) \simeq l\left(\frac{1}{2}\sqrt{\frac{u_A}{r_A}} + \frac{1}{2}\sqrt{\frac{u_B}{r_B}}\right). \tag{24}$$

Then, using the heterogeneity parameters from Eq. (12) in Eq. (24), we obtain

$$R(\lambda, \gamma \to 0) \simeq \frac{1}{2}\left(\sqrt{\frac{\alpha_u}{\alpha_r}} + \sqrt{\frac{\alpha_r}{\alpha_u}}\right). \tag{25}$$

Mathematically, it is clear that the function $R(\lambda, \gamma \to 0) > 1$ at all values of $\alpha_u \neq \alpha_r$, as also observed in Fig. 4(a). One can easily find that $R(\lambda) = 1$ only when the dimensionless parameters are equal, i.e., for $\alpha_u = \alpha_r$. Physically, this means that due to heterogeneity, the communication lengths in one of the macrostates become larger than in the static case, effectively increasing the overall communication length. This explains the dynamic behavior for small γ. For large fluctuation rates ($\gamma \to \infty$), the system can be viewed as a homogeneous one with effective migration and death rates,

$$u_{eff} = \frac{1}{2}(u_A + u_B), \quad r_{eff} = \frac{1}{2}(r_A + r_B). \tag{26}$$

Then, the communication length in this limit can be written as

$$\lambda \simeq l\sqrt{\frac{u_A + u_B}{r_A + r_B}}, \tag{27}$$

which leads to

$$R(\lambda, \gamma \to \infty) \simeq \sqrt{\frac{\alpha_u + \frac{1}{\alpha_u}}{\alpha_r + \frac{1}{\alpha_r}}}. \tag{28}$$

This expression can be larger or smaller than unity depending on the specific values of the heterogeneity parameters. One should note that the function $f(x) = x + 1/x$ (for $x > 0$) is always decreasing for $0 < x < 1$ and always increasing for $x > 1$, with the minimum being achieved at $x = 1$. Then, there are four possible situations: (1) for $\alpha_u > 1$ and $\alpha_r > 1$, the parameter $R(\lambda) > 1$ for $\alpha_u > \alpha_r$ and $R(\lambda) < 1$ for $\alpha_u < \alpha_r$; (2) for $\alpha_u < 1$ and $\alpha_r < 1$, the parameter $R(\lambda) > 1$ for $\alpha_u < \alpha_r$ and $R(\lambda) < 1$ for $\alpha_u > \alpha_r$; (3) for $\alpha_u > 1$ and $\alpha_r < 1$, the parameter $R(\lambda) > 1$ for $\alpha_u > 1/\alpha_r$ and $R(\lambda) < 1$ for $\alpha_u < 1/\alpha_r$; and (4) for $\alpha_u < 1$ and $\alpha_r > 1$, the parameter $R(\lambda) > 1$ for $\alpha_u < 1/\alpha_r$ and $R(\lambda) < 1$ for $\alpha_u > 1/\alpha_r$. Importantly, the parameter $R(\lambda) = 1$ when $\alpha_u = \alpha_r^{\pm 1}$. This corresponds to the situation when dynamic fluctuation modifies the migration and death rates in each macrostate to the same degree, leading to unchanged communication length because $\lambda \sim \sqrt{u/r}$. In these special cases, the dynamic fluctuations do not affect the communication length at all, despite observable dynamic rearrangements in the system. All these results are clearly illustrated in Fig. 4(b).

C. Catalytic cooperativity in the systems with multiple macrostates

Our theoretical analysis of the effect of dynamic restructuring on catalytic cooperativity has concentrated so far on the simplest situation with only two macrostates. However, it is more realistic to expect transitions between multiple structural conformations of the single NP. This also raises the question of whether the results obtained in our two-macrostate approach will survive if more macrostates are taken into account.

To test the role of the number of macrostates in dynamic restructuring, we performed Monte Carlo computer simulations to evaluate the communication distances and lifetimes for a more realistic situation. It was assumed that the single nanorod can experience 50 different macrostates. In each of them, we randomly picked the migration and death rates from Gaussian distributions that are centered around homogeneous migration and death rates utilized in previous theoretical analysis of catalytic cooperativity.[20] Further simulation details are provided in the supplementary material.

The results of our computer simulations are presented in Fig. 5. One can see from Fig. 5(a) that dynamic transitions that influence only the migration rates (red curve) do not affect the communication times, but those that modify the death rates (blue and green curves) strongly modify the memory lifetimes. In these cases, the memory times always decrease as a function of the dynamic fluctuation rate. This fully agrees with our analytical calculations for the two-macrostate model [compare with Fig. 2(a)]. For the communication lengths [Fig. 5(b)], we observe that the effect of the fluctuation rate depends on the degree of changes in migration and death rates due to dynamic fluctuations, producing an increase or decrease in the communication length. These results generally agree with the predictions and trends for the two-macrostate systems, further supporting our theoretical method. It is important to note that the two-macrostate

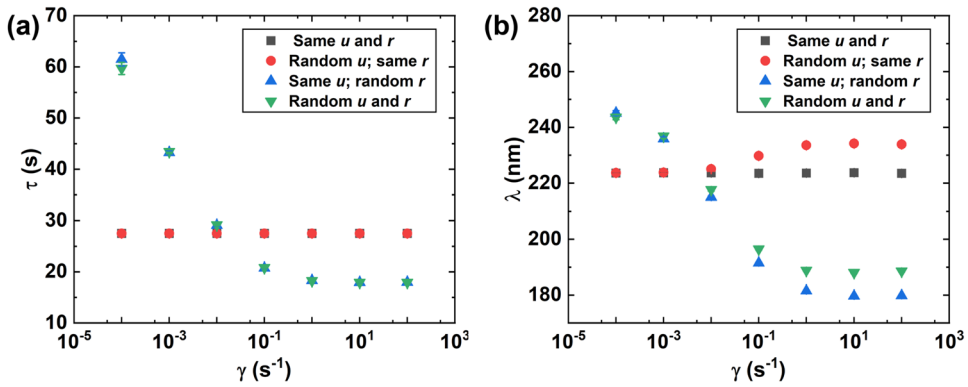

FIG. 5. (a) Temporal memory, τ, and (b) communication distance, λ, for the systems with multiple macrostates as a function of the dynamic fluctuation rate. The results are obtained from computer simulations. A single nanorod is allowed to dynamically transform between 50 macrostates with equal rate γ. The nanorod is divided into multiple segments of length l = 50 nm, and the migration and death rates in each macrostate are randomly picked from respective Gaussian distributions, with the average value of death rates as $r = 0.036\,36\ s^{-1}$ and migration rates as $u = 0.736\ s^{-1}$, which are used in Ref. 20 for the static case of *Pd* nanorods. The standard deviations about the mean values are $\sigma_r = 0.05\ s^{-1}$ and $\sigma_u = 0.5\ s^{-1}$, respectively. The creation rate of a hole is $k = r = 0.036\,36\ s^{-1}$.

approach allows us to better explain the underlying physics of how the dynamic restructuring affects the catalytic cooperativity.

In single-molecule experiments, the quantities τ and λ have been determined by analyzing a well-known statistical parameter called Pearson's cross correlation coefficient (PCC or ρ_{τ_i,τ_j}).[18] This quantity exhibited an exponential decay with respect to the average time separation $(\Delta t_{i,j})$ between successive product formation events as well as the distance separation $(\Delta x_{i,j})$ of any two segments i and j of a single nanorod. The respective decay constants provided the quantities τ and λ, respectively. As discussed in detail within the supplementary material, we performed multiple-particle Monte Carlo computer simulations to mimic this experimental analysis by monitoring the hole-creation events on a single nanorod. The characteristic exponential decay of the PCC values is observed for all the simulated situations, further supporting our theoretical approach.

IV. SUMMARY AND CONCLUSIONS

In this paper, we investigated the effect of dynamic restructuring of single nanoparticle catalysts on catalytic cooperativity. The analysis was performed by extending the original discrete-state stochastic approach for homogeneous systems. In our theoretical method, dynamic restructuring is viewed as a set of stochastic transitions between different macrostates characterized by different dynamic properties of charged holes that are known to be responsible for catalytic cooperativity. By considering the simplest model with two macrostates, the dynamics of catalytic cooperativity are explicitly evaluated. It is found that increasing the speed of dynamic fluctuations always decreases the communication times, while the effect on communication length depends on specific relations between transition rates. Physical–chemical arguments to explain these observations are presented.

The effect of dynamic structuring on the lifetime and communication distance relative to our original model for a homogeneous system can be successfully quantified using the specific dimensionless parameters $R(\tau)$ and $R(\lambda)$, respectively. These parameters allow us to extend our theoretical analysis to more realistic scenarios, as demonstrated by the example of the redox reaction of resazurin disproportionation on *Pd* nanorods, as performed by Zou *et al.*[18] The assumption of equal fluctuation rates $(\gamma_A = \gamma_B = \gamma)$ and the presence of only two macrostates were introduced to simplify our calculations and provide clear insights into the underlying dynamics. However, the strength of our method lies in its generality, as our theoretical framework can be extended to cases with varying fluctuation rates between macrostates. For example, in Fig. S2, we show the variation in the dimensionless parameters $R(\tau)$ and $R(\lambda)$ for the systems with non-equal fluctuation rates, demonstrating the flexibility of our approach. Importantly, experimental evidence supports the effective two-macrostate picture. Distinct transitions between resting and active states have been observed in *Au* nanoparticles during butadiene hydrogenation,[27] and two types of restructuring processes were reported on Au nanoparticles while they catalyze the reduction of *p*-nitrophenol.[30] These observations align well with our simplified model, further validating its relevance to realistic catalytic systems. We have also extended our theoretical analysis to include cases where dynamic restructuring leads to multiple macroscopic states (see Fig. 5), and the results remain qualitatively consistent with those derived from the simpler two-state model. This suggests that our simplified assumptions are reasonable while still capturing the essential dynamics of metal nanorods. Thus, the presented theoretical method clarifies the microscopic picture of how dynamic restructuring influences the phenomena of catalytic cooperativity.

In particular, our theory predicts that faster dynamic fluctuations reduce both communication lengths and lifetimes, but they also enhance the strength of cooperative effects, especially when the heterogeneity in death rates is greater than that in migration rates. These insights offer potential strategies to improve catalytic efficiency. For example, increasing the density of traps or incorporating the processes that accelerate hole removal (i.e., increasing the death rates) could lead to faster communication and reaction times, thereby enhancing catalyst performance. In addition, photochemical

methods could be employed to fine-tune these transition rates. By controlling the spatial arrangement of active sites on the nanoparticle surface, it may be possible to introduce favorable changes that optimize these cooperative effects, thereby designing more efficient catalytic systems; see also Ref. 20.

Although the presented theoretical method provides a physically consistent picture of the role of dynamic fluctuations for catalytic cooperativity, it is crucial to critically analyze its limitations. This theoretical approach hypothesizes that each chemical reaction occurring on an active site produces a charged hole. Afterward, this hole diffuses on the nanoparticle surface until it disappears. Therefore, only the hole's creation rate directly relates to the reaction under consideration. Other parameters such as migration and death rates are tied to the hole's dynamic behavior and reflect the system's broader macrostate rather than being directly related to specific chemical processes. Our model does not address the exact microscopic mechanisms responsible for hole creation, nor does it capture quantum-mechanical details of the underlying processes. These aspects are beyond the scope of our current theoretical framework, and their inclusion would require more detailed electronic structure information.[20]

In addition, our strongest assumption is that dynamic restructuring does not change the uniform distribution of active sites along the catalytic nanoparticle. Realistically, one expects changes in both the dynamic properties of charged holes and in the number of active sites per unit length of the nanocatalyst. It can be noted, however, that the impact of spatial variations for nanocatalysts has already been theoretically probed by us, but it was only studied for stationary systems without dynamic fluctuations.[24] This means that it will be important to investigate catalytic cooperativity when both spatial and dynamic fluctuations are happening, and this might lead to some new phenomena. Another limitation of our study is that it concentrated only on effective one-dimensional systems, while many nanoparticles deviate from this simple geometry. In addition, our theoretical study did not take into account the finite-size effects of nanocatalysts. However, despite these reservations, the proposed theoretical method provides a fully quantitative physical–chemical analysis of catalytic cooperativity that can be further tested in experiments and more advanced theoretical studies.

SUPPLEMENTARY MATERIAL

See the supplementary material for the calculations to solve first passage time distributions, determine steady-state probabilities, details of the Monte Carlo computer simulations, Pearson's cross correlation coefficient analysis, and additional microscopic arguments in support of our theoretical findings.

ACKNOWLEDGMENTS

B.P. acknowledges IISER Pune and the Prime Minister Research Fellowship (PMRF), India, for the funding and fellowship. A.K. was supported by the Welch Foundation (Grant No. C-1559) and by the NSF (Grant No. CHE-2246878). S.C. acknowledges the support from SERB Power Fellowship (Grant No. SPF/2022/000155).

AUTHOR DECLARATIONS

Conflict of Interest

The authors have no conflicts to disclose.

Author Contributions

Srabanti Chaudhury and Anatoly Kolomeisky contributed equally to this paper.

Bhawakshi Punia: Formal analysis (equal); Investigation (equal); Methodology (equal); Validation (equal). **Srabanti Chaudhury**: Conceptualization (equal); Formal analysis (equal); Funding acquisition (equal); Methodology (equal); Project administration (equal); Supervision (equal); Validation (equal); Writing – original draft (equal); Writing – review & editing (equal). **Anatoly Kolomeisky**: Conceptualization (equal); Funding acquisition (equal); Investigation (equal); Methodology (equal); Project administration (equal); Writing – original draft (equal); Writing – review & editing (equal).

DATA AVAILABILITY

The data that support the findings of this study are available within the article and its supplementary material.

REFERENCES

[1] R. J. Farrauto, L. Dorazio, and C. H. Bartholomew, *Introduction to Catalysis and Industrial Catalytic Processes* (John Wiley & Sons, 2016).
[2] G. A. Somorjai and Y. Li, *Introduction to Surface Chemistry and Catalysis* (John Wiley & Sons, 2010).
[3] E. Roduner, "Understanding catalysis," Chem. Soc. Rev. **43**, 8226–8239 (2014).
[4] J. R. Ross, *Heterogeneous Catalysis: Fundamentals and Applications* (Elsevier, 2011).
[5] I. Fechete, Y. Wang, and J. C. Védrine, "The past, present and future of heterogeneous catalysis," Catal. Today **189**, 2–27 (2012).
[6] R. Schlögl, "Heterogeneous catalysis," Angew. Chem., Int. Ed. **54**, 3465–3520 (2015).
[7] L. Liu and A. Corma, "Metal catalysts for heterogeneous catalysis: From single atoms to nanoclusters and nanoparticles," Chem. Rev. **118**, 4981–5079 (2018).
[8] D. Astruc, "Introduction: Nanoparticles in catalysis," Chem. Rev. **120**, 461 (2020).
[9] J. Spivey, *Metal Nanoparticles for Catalysis: Advances and Applications* (Royal Society of Chemistry, 2014).
[10] B. Roldan Cuenya, "Metal nanoparticle catalysts beginning to shape-up," Acc. Chem. Res. **46**, 1682–1691 (2013).
[11] K. An and G. A. Somorjai, "Size and shape control of metal nanoparticles for reaction selectivity in catalysis," ChemCatChem **4**, 1512–1524 (2012).
[12] K. P. Janssen, G. De Cremer, R. K. Neely, A. V. Kubarev, J. Van Loon, J. A. Martens, D. E. De Vos, M. B. Roeffaers, and J. Hofkens, "Single molecule methods for the study of catalysis: From enzymes to heterogeneous catalysts," Chem. Soc. Rev. **43**, 990–1006 (2014).
[13] M. R. Decan, S. Impellizzeri, M. L. Marin, and J. C. Scaiano, "Copper nanoparticle heterogeneous catalytic 'click' cycloaddition confirmed by single-molecule spectroscopy," Nat. Commun. **5**, 4612 (2014).
[14] H. Shen, X. Zhou, N. Zou, and P. Chen, "Single-molecule kinetics reveals a hidden surface reaction intermediate in single-nanoparticle catalysis," J. Phys. Chem. C **118**, 26902–26911 (2014).
[15] T. Chen, Y. Zhang, and W. Xu, "Single-molecule nanocatalysis reveals catalytic activation energy of single nanocatalysts," J. Am. Chem. Soc. **138**, 12414–12421 (2016).
[16] X. Qu, B. Zhao, W. Zhang, J. Zou, Z. Wang, Y. Zhang, and L. Niu, "Single-molecule nanocatalysis reveals the kinetics of the synergistic effect based on single-AuAg bimetal nanocatalysts," J. Phys. Chem. Lett. **13**, 830–837 (2022).

[17]W. Xu, J. S. Kong, Y.-T. E. Yeh, and P. Chen, "Single-molecule nanocatalysis reveals heterogeneous reaction pathways and catalytic dynamics," Nat. Mater. **7**, 992–996 (2008).
[18]N. Zou, X. Zhou, G. Chen, N. M. Andoy, W. Jung, G. Liu, and P. Chen, "Cooperative communication within and between single nanocatalysts," Nat. Chem. **10**, 607–614 (2018).
[19]R. Ye, X. Mao, X. Sun, and P. Chen, "Analogy between enzyme and nanoparticle catalysis: A single-molecule perspective," ACS Catal. **9**, 1985 (2019).
[20]B. Punia, S. Chaudhury, and A. B. Kolomeisky, "Microscopic mechanisms of cooperative communications within single nanocatalysts," Proc. Natl. Acad. Sci. U. S. A. **119**, e2115135119 (2022).
[21]A. Furube, T. Asahi, H. Masuhara, H. Yamashita, and M. Anpo, "Charge carrier dynamics of standard TiO_2 catalysts revealed by femtosecond diffuse reflectance spectroscopy," J. Phys. Chem. B **103**, 3120–3127 (1999).
[22]A. Studer and D. P. Curran, "The electron is a catalyst," Nat. Chem. **6**, 765–773 (2014).
[23]Q. Hu, X. Yu, S. Gong, and X. Chen, "Nanomaterial catalysts for organic photoredox catalysis-mechanistic perspective," Nanoscale **13**, 18044–18053 (2021).
[24]B. Punia, S. Chaudhury, and A. Kolomeisky, "How heterogeneity affects cooperative communications within single nanocatalysts," J. Phys. Chem. Lett. **14**, 8227–8234 (2023).
[25]P. Chen, X. Zhou, N. M. Andoy, K.-S. Han, E. Choudhary, N. Zou, G. Chen, and H. Shen, "Spatiotemporal catalytic dynamics within single nanocatalysts revealed by single-molecule microscopy," Chem. Soc. Rev. **43**, 1107–1117 (2014).
[26]X. Liu, T. Chen, P. Song, Y. Zhang, and W. Xu, "Single-molecule nanocatalysis of pt nanoparticles," J. Phys. Chem. C **122**, 1746–1752 (2018).
[27]D. James Martin, D. Decarolis, Y. I. Odarchenko, J. J. Herbert, T. Arnold, J. Rawle, C. Nicklin, H.-G. Boyen, and A. M. Beale, "Reversible restructuring of supported au nanoparticles during butadiene hydrogenation revealed by *operando* GISAXS/GIWAXS," Chem. Commun. **53**, 5159–5162 (2017).
[28]C. Vogt, F. Meirer, M. Monai, E. Groeneveld, D. Ferri, R. A. van Santen, M. Nachtegaal, R. R. Unocic, A. I. Frenkel, and B. M. Weckhuysen, "Dynamic restructuring of supported metal nanoparticles and its implications for structure insensitive catalysis," Nat. Commun. **12**, 7096 (2021).
[29]X.-Y. Li, P. Ou, X. Duan, L. Ying, J. Meng, B. Zhu, and Y. Gao, "Dynamic active sites in situ formed in metal nanoparticle reshaping under reaction conditions," JACS Au **4**, 1892 (2024).
[30]S. Wunder, Y. Lu, M. Albrecht, and M. Ballauff, "Catalytic activity of faceted gold nanoparticles studied by a model reaction: Evidence for substrate-induced surface restructuring," ACS Catal. **1**, 908–916 (2011).
[31]B. Zhu, J. Meng, W. Yuan, X. Zhang, H. Yang, Y. Wang, and Y. Gao, "Reshaping of metal nanoparticles under reaction conditions," Angew. Chem., Int. Ed. **59**, 2171–2180 (2020).
[32]J. Shin and A. B. Kolomeisky, "Asymmetry of forward/backward transition times as a non-equilibrium measure of complexity of microscopic mechanisms," J. Chem. Phys. **153**, 124103 (2020).